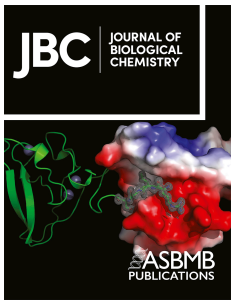

Melatonin-mediated cGAS-STING signal in senescent macrophages promote TNBC chemotherapy resistance and drive the SASP

Xiaoqiang Zhang, Minyu Zhuang, Hongfei Zhang, Yanhui Zhu, Junzhe Yang, Xian Wu, Xiafei Yu, Jing Tao, Xiaoan Liu

PII: S0021-9258(25)00287-X

DOI: https://doi.org/10.1016/j.jbc.2025.108438

Reference: JBC 108438

To appear in: *Journal of Biological Chemistry*

Received Date: 11 October 2024

Revised Date: 8 March 2025

Accepted Date: 18 March 2025

Please cite this article as: Zhang X, Zhuang M, Zhang H, Zhu Y, Yang J, Wu X, Yu X, Tao J, Liu X, Melatonin-mediated cGAS-STING signal in senescent macrophages promote TNBC chemotherapy resistance and drive the SASP, *Journal of Biological Chemistry* (2025), doi: https://doi.org/10.1016/j.jbc.2025.108438.

Melatonin-mediated cGAS-STING signal in senescent macrophages promote TNBC chemotherapy resistance and drive the SASP

Xiaoqiang Zhang[1,2#], Minyu Zhuang[2#], Hongfei Zhang[3#], Yanhui Zhu[2], Junzhe Yang[2], XianWu[2], Xiafei Yu[2], Jing Tao[4]*, Xiaoan Liu[2]**

[1] Zhejiang Cancer Hospital, Hangzhou Institute of Medicine (HIM), Chinese Academy of Sciences, Hangzhou, Zhejiang 310022, China.

[2] Breast Disease Center, The First Affiliated Hospital of Nanjing Medical University, 300 Guangzhou Road, Nanjing, Jiangsu 210029, P.R. China

[3] Department of Ultrasound in Medicine, Second Affiliated Hospital, Zhejiang University School of Medicine, Zhejiang, China.

[4] Department of General Surgery, The Fourth Affiliated Hospital of Nanjing Medical University, Nanjing Medical University, Nanjing, Jiangsu, China.

#Xiaoqiang Zhang, Minyu Zhuang and Hongfei Zhang contributed equally to this work

* Xiaoan Liu, Jing Tao and Xiafei Yu are the corresponding authors of this work

Correspondence

Xiaoan Liu, Breast Disease Center, The First Affiliated Hospital of Nanjing Medical University, 300 Guangzhou Road, Nanjing, Jiangsu 210029, P.R. China

Email: liuxiaoan@126.com

Jing Tao, Department of General Surgery, The Fourth Affiliated Hospital of Nanjing Medical University, Nanjing Medical University, Nanjing, Jiangsu, China.

Email: chnn123@163.com

Xiafei Yu, Breast Disease Center, The First Affiliated Hospital of Nanjing Medical University, 300 Guangzhou Road, Nanjing, Jiangsu 210029, P.R. China

Email: 347311312@qq.com

Abstract

The build-up of senescent cells in tissues is a key indicator of aging, associated with negative prognosis and therapy resistance. Despite immune dysfunction related to aging, also known as immunosenescence, is recognized as a factor in this process, the exact mechanisms are still unclear. In this study, we reported that melatonin deficiency accelerated macrophage senescence in triple-negative breast cancer (TNBC), whereas, melatonin could defend macrophages against senescence through the Nfatc1-Trim26-cgas-Sting pathway. Mechanistically, melatonin enhanced the nuclear translocation of Nfatc1 and elevated Trim26 transcription levels. Trim26, functioning as an E3 ligase, ubiquitinates cgas, thereby inhibiting the activation of the cgas-Sing pathway and consequently preventing cell senescence. Conversely, melatonin deficiency induced cgas-Sting pathway activation to promote macrophage aging. Our results show that melatonin inhibited macrophage senescence and improved chemotherapy responsiveness, with further enhancement when combined with the cgas inhibitor (G150). Overall, our findings indicated that melatonin protects macrophages from immunosenescence, suggesting its therapeutic potential for enhancing chemotherapy response.

Keywords

TNBC, chemotherapy, melatonin, macrophage, senescence

Introduction

Breast cancer (BC) stands as a prominent cause of cancer-related mortality in women, accounting for 32% of all instances[1], and is categorized into three primary subtypes: luminal (expresses the estrogen receptor), HER2-enrich and triple-negative breast cancer (TNBC)[2, 3]. Despite recent breakthroughs, clinical barriers such as metastasis, recurrence and chemoresistance continue to persist[4]. While TNBC often exhibits initial heightened responsiveness to chemotherapy when compared to other subtypes, a substantial proportion of patients may develop drug resistance after receiving a period of treatment. This phenomenon restricts available regimens for subsequent therapies and leads to unfavorable clinical outcomes. The molecular mechanisms driving this occurrence still remain ambiguous. Furthermore, the intricate relationship between tumor-associated macrophages (TAMs) and cancer cells, which facilitates resilient adjustment for survival in a challenging chemotherapy environment, remains largely unexplored.

Cellular senescence is known as a steady stoppage of the cell cycle combined with a changed level of gene expression[5, 6]. Numerous chronic cellular stressors have been shown to be the cause of cellular senescence, such as the accumulation of unrepaired DNA damage, oncogene activation, telomere attrition, and exposure to reactive oxygen species and cytotoxic substances[7, 8]. Senescence-associated secretory phenotype (SASP) is a characteristic of senescent cells that causes them to release more pro-inflammatory cytokines, which in turn cause chronic inflammation. In terms of molecular, the senescent state is typically identified by the presence of cyclin-dependent kinase inhibitors, notably $p16^{INK4a}$ from the Cdkn2a gene, and elevated level of senescence-associated β-galactosidase (SA-β-gal).

The immune system possesses mechanisms to detect and eliminate senescent cells. Once senescent cells are destroyed by natural killer (NK) cells or cytotoxic T cells, chemokines, including C-C motif chemokine ligand 2 (CCL2) and CXC motif chemokine ligand 14 (CXCL14), are secreted, attracting macrophages to phagocytose

the dead cells[9, 10]. However, as chemotherapy progresses, the immune system is compromised, leading to reduction in both qualitative responses and cell numbers[11, 12], and consequently, impaired capacity in removing senescent cancer cells[13]. Immune cells are also susceptible to senescence, a state that contributes to tumor progression primarily through the secretion of SASP[13, 14]. Macrophages expressing p16^{INK4a}[15] in tumorigenic lungs produce various pro-tumorigenic SASP factors, which may play crucial roles in mediating paracrine pro-tumorigenic effects. Nevertheless, elucidating the specific factors that drive immune cell senescence and the detailed molecular mechanisms by which these senescent cells regulate tumor progression remains a complex and challenging endeavor.

In this research, we examined the role of melatonin deficiency in contributing to chemoresistance and accelerating the aging process in mice. Our research revealed that the observed phenotype is predominantly due to a compromised melatonin-Trim26-cgas pathway. This deficiency heightens macrophage vulnerability to senescence, thereby diminishing their capacity to sustain innate immune functionality. Significantly, our data indicated that enhancing melatonin levels within TAMs substantially improved chemotherapy responsiveness. These results implied that increasing melatonin secretion could represent a viable therapeutic approach for TNBC treatment.

Results

Senescent macrophages are correlated with chemoresistance and adverse prognosis

Chemotherapy is known to lead to the accumulation of senescent cells[16]. Senescent macrophages have been reported to be critical in tumor progression, but their role in chemotherapy remains unclear[15, 17]. scRNA-seq (Single-cell RNA sequencing) has been rigorously validated as a powerful methodology for unraveling tumor heterogeneity and evaluating the complex interactions within the tumor microenvironment. To provide a comprehensive perspective on how variations within

the tumor microenvironment influence chemotherapy responsiveness, we executed scRNA-seq on biopsies from TNBC patients obtained prior to chemotherapy. A total of 5,669 cells from two patients, meeting stringent quality control standards, were included in the subsequent phase of investigation. Using established markers, the cells revealed 12 distinct phenotypic types, with the UMAP plot indicating subcluster distributions across both patients (Figure 1A). The scRNA-seq analysis indicated a higher prevalence of macrophage cells and a lower frequency of T cells in the Non-res group (Figure 1B). We performed KEGG pathway analysis in the two groups of single-cell data. The results showed that the Non-res group were significantly associated with cell senescence, cell adhesion, phagosomes, and PPAR signaling pathways (Figure 1C). Cellular senescence is a unique cell state marked by a halt in replication, triggered by various external and internal stresses[18]. To investigate the potential role of aging in the accumulation of macrophages in Non-res patient, we examined the expression of senescence-associated genes across various cell types. The results indicated that macrophages exhibited notably high expression of IL-1β, CXCL8, CDKN1A, and TNF (Figure 1D). Subsequently, we performed a comparative assessment of the expression levels of senescence-related genes between Non-res and Res patient. Ultimately, as anticipated, the Non-res patient, exhibiting elevated senescence gene expression in TAMs. In contrast, the Res patient showed lower senescence gene expression (Figure 1E,1F). To further explore the role of senescent macrophages in response to TNBC chemotherapy, we collected 30 TNBC patients undergoing neoadjuvant chemotherapy in our hospital and their clinicopathological characteristics are shown in Supplementary Table 1. The patients were assigned to two groups, response (Res) and non-response (Non-res) based on their responsiveness to chemotherapy evaluated by postoperative pathology. We found that the frequency of $CD68^{+}p16^{+}$ cells differed substantially between Res and Non-res malignant tissues. Tumors enriched with $CD68^{+}p16^{+}$ cells exhibited enhanced chemoresistance (Figure 1G). Based on the TCGA database, age is a risk factor affecting the poor prognosis of TNBC patients undergoing chemotherapy

(Figure 1H). Metabolic programming is heavily dependent on the tumor microenvironment[19]. Therefore, we measured the expression levels of aging-related metabolites in the peripheral blood of patients by using ELISA assays, and discovered that melatonin levels of the Res group were considerably higher than the Non-res group, and other metabolite levels did not vary significantly (Figure 1I). We further discovered that the melatonin levels in tumor-associated macrophages (TAMs) were increased in Res group (Figure 1J). Additionally, it was revealed that p16 staining intensity in tumor tissues was inversely correlated with melatonin levels in TAMs (Figure 1K). According to the Kaplan–Meier survival curve and multivariate cox regression analysis, age contributes to the prognosis of TNBC patients as a risk factor (Supplementary Figure 1A, 1B). These findings highlighted that senescent macrophages are linked to chemoresistance and their accumulation signals a poor prognosis in TNBC patients.

Melatonin improves chemotherapy responsiveness through inhibiting macrophage senescence

To further clarify the role of melatonin in chemotherapy-related macrophage senescence, we pre-treated bone marrow derived macrophages (BMDMs) isolated from BALB/c mice with melatonin. Following a 48-hours exposure to varying melatonin concentrations (0/10/50/100μM), BMDMs were then treated with 1μM doxorubicin (DOX) for 24 hours (Figure 2A). The quantitative results of SA-β-gal staining showed SA-β-gal^{+} cells were decreased in a concentration-dependent manner (Figure 2B). Similarly, qRT-PCR confirmed that Il-6 and p21 mRNA expression was notably decreased with increasing melatonin concentrations (Figure 2C). Taken together, we initially verified that melatonin could inhibit macrophage senescence and chose 50μM of melatonin as the optimum concentration for the subsequent experiments. A declined expression of senescence related factors, including Il-6, Il-8, Il-1α, p21 and p53, was observed in melatonin group (Figure 2D,2E). Macrophages exposed to melatonin exhibited a higher oxygen consumption rate (OCR) and increased maximum respiratory

capacity. Accordingly, the inhibition of glycolysis was confirmed by the simultaneous reduction of baseline extracellular acidification rate (ECAR) in response to melatonin stimulation (Figure 2F). It is known that melatonin acts primarily through membrane receptors: MT1 or MT2[20]. To further measure the anti-senescence effect of melatonin, luzindole (the blocker of both MT1 and MT2) or 4-P-PDOT (the blocker of MT2) was added at one hour prior to melatonin treatment. The inhibitors of melatonin membrane receptor activity could reverse the inhibitory effect of melatonin on chemotherapy-related macrophage senescence, as reflected by the high proportion of SA-β-gal$^+$ cells and greatly elevated expression of SASP factors (Figure 2G-2I, Supplementary Figure 1C-1E). Next, the effects of melatonin on tumor-associated macrophage senescence and chemotherapy sensitivity were investigated in vivo. For the tumor formation, 4T1 cells were injected into the mammary fat pad of BALB/c mice. When tumors grew to a volume of 100 mm^3, the mice were subjected to DMSO or melatonin every three days, combined with DOX treatment once per week for four weeks (Figure 2J). Mice treated with melatonin showed a better response to the DOX treatment, as revealed by the decreased tumor volume (Figure 2K). Consistently, the melatonin group had a lower Ki67 proliferation index and more TUNEL-positive cells (Figure 2L). In contrast to the DMSO group, the tumor tissue injected with melatonin recruited less F4/80$^+$p16$^+$ cells, which in consistent with our previous in vitro result (Figure 2M). Together, these results demonstrated that melatonin can improve chemotherapeutic responsiveness by inhibiting chemotherapy-induced macrophage senescence.

Melatonin inhibits macrophage senescence by boosting the transcription of Trim26 through the induction of Nfatc1 in macrophages

We next performed RNA sequencing (RNA-seq) of tumor-associated macrophages (TAMs) isolated from tumors with or without melatonin treatment (the specific mouse model method was shown in Figure 2J). Heatmap of the RNA-seq data revealed that Trim26 was significantly upregulated in the melatonin treatment group ($p \leq 0.05$; |log

(fold change) | ≥ 0.5) (Figure 3A). Gene set enrichment analysis (GSEA) of melatonin treatment group compared with DMSO group showed downregulation of senescence-related pathways (Figure 3B,3C). Moreover, according to qRT-PCR analysis, Trim26 mRNA expression was increased in the TAMs of the melatonin-treated group in line with the RNA-seq data (Figure 3D). TRIM26, an important member of the E3 ubiquitin ligase family, has been implicated in the development and incidence of various tumors. For instance, TRIM26 and USP39 balanced the ZEB1 ubiquitination level to regulate the progression of hepatocellular carcinoma[21]. Additionally, TRIM26 accelerated glioma through PLK1/TRIM26/GPX4 axis[22]. To further determine the effect of Trim26 in TNBC, we constructed short hairpin RNA (shRNA) silencing of Trim26. The efficiency of knockdown was validated at mRNA levels (Supplementary Figure 1F). We chose shTrim26-1 (called shTrim26 for short) for the subsequent experiments. BMDMs isolated from BALB/c mice were pre-treated with 50μM melatonin for 48 hours prior to DOX treatment, with prior transfection of shTrim26 or shNC. qRT-PCR analyses showed that knockdown of Trim26 enhanced the mRNA expression of Il-6, Il-1α, p21 and p53 (Figure 3E). Also, notably increased SA-β-gal staining was observed in BMDMs transfected with shTrim26 (Figure 3F). Overexpression of Trim26 (shRNA-resistant) in Trim26 knockdown cells reduces BMDM senescence, as indicated by SA-β-gal staining. (Supplementary Figure 1G). To verify the role of Trim26 in vivo, a mouse tumorigenicity model was generated and clodronate liposome was used for the macrophage depletion. BALB/c mice received macrophage adoptive through injected BMDM-shTrim26 or BMDM-shNC intravenously. When tumors grew to a volume of 100 mm^3, the mice were subjected to melatonin and DOX treatment. In contrast to the control group, Mel+shTrim26 group mice exhibited a poorer response to DOX treatment, as reflected by the increased tumor volume, decreased TUNEL-positive cells and elevated the cell proliferation marker Ki67 expression (Figure 3G-3I). We also observed the induction of $F4/80^+p16^+$ cells in the Mel+shTrim26 group (Figure 3J). These in vivo findings further evaluated that Trim26 knockdown could

reverse the inhibitory effect of melatonin on macrophage senescence and decrease chemotherapy responsiveness, which indicated that melatonin act through Trim26. To explore how melatonin induces Trim26 expression, five candidates of Trim26-promoter-binding transcription factors were predicted using NCBI and Jaspar databases. Next, luciferase plasmids with the full Trim26 promoter region or truncated versions were created. We found that Nfatc1, Rxra, and Nr2f6 induced the activation of the full Trim26 promoter, with Nfatc1 possessing the greatest change fold (Figure 3K). Whereas in BMDMs treated with melatonin, only Nfatc1 overexpression activated the transcription of Trim26 (Figure 3L). Consistent with these results, qRT-PCR confirmed that Trim26 upregulation in Nfatc1-infected BMDMs, indicating that Nfatc1 was the most probable transcription factor regulating Trim26 expression (Figure 3M). To verify this regulation, potential Nfatc1-binding sites in the Trim26 promoter were determined using Jaspar and two putative binding sites were observed (Figure 3N). The luciferase experiment combined with site-directed mutagenesis revealed that binding sites 2 in the Trim26 promoter-induced Nfatc1-reduced promoter activity in BMDMs with Nfatc1 knockdown. The occupancy at the binding sites 2 of Trim26 promoters was further confirmed by ChIP tests (Figure 3O,3P). Taken together, melatonin regulated Trim26 transcription through Nfatc1 and the binding sites 2 was critical for activating Trim26 transcription. The localization of Nfatc1 between cytoplasmic and nuclear is a dynamic process, ensuring a balanced signaling activation. We thus questioned whether melatonin is participated in the regulation of Nfatc1 distribution. Administration of BMDMs with melatonin led to a pronounced augmentation of Nfatc1 in the nuclear compartment, coupled with a marked reduction in its cytoplasmic localization (Figure 3Q, 3R). To further verify the connection between melatonin and Nfatc1, we conducted coimmunoprecipitation assays using biotin-labeled followed by pull-down with streptavidin beads. Our results found a strong interaction between melatonin and Nfatc1 (Figure 3S). These data suggested that melatonin facilitated Nfatc1 nuclear distribution, and then promoted Nfatc1-induced Trim26 transcription.

Trim26 interacts with and degrades cgas

Immunoprecipitation (IP) and LC-MS/MS screening were conducted to investigate the putative interacting proteins of Trim26 in macrophages, only the cgas protein is closely related to senescence among the top ten enriched proteins. Hence, we hypothesized that cgas might be the potential binding protein downstream of Trim26 (Figure 4A). Endogenous and exogenous coimmunoprecipitation (Co-IP) assays showed the indirect interaction between Trim26 and cgas (Figure 4B-4D). GST pull-down test was then performed to verify the direct interaction between Trim26 and cgas in macrophages (Figure 4E). Confocal microscopy also verified the co-localization of Trim26 and cgas (Figure 4F). Following Trim26 knockdown, macrophages showed an increase in endogenous cgas protein levels (Figure 4G). Overexpression of Trim26 (shRNA-resistant) in Trim26 knockdown cells decreases cgas expression, as shown by Western blot analysis (Supplementary Figure 1H). The reduction in cgas protein levels caused by Trim26 overexpression was reversed after the treatment of proteasome inhibitor MG132, whereas the lysosome inhibitor chloroquine (CQ) could not exert the same effect. The qRT-PCR result indicated that Trim26 had no effect on the RNA levels of cgas, suggesting that Trim26 regulated cgas at post-transcriptional level through the ubiquitin-proteasome pathway rather than the transcript level (Figure 4H-4J). Furthermore, a cycloheximide chase experiment revealed that the half-life of cgas was prolonged in Trim26-downregulated cells compared to those overexpressing Trim26 (Figure 4K). The functional role of Trim26 as cgas ubiquitinase was examined by immunoblot analysis using an anti-Myc antibody, and the total amount of cellular ubiquitin was determined by immunoprecipitation using an anti-HA antibody. These analyses revealed that Trim26 uses ubiquitination modification to control cgas expression, as Trim26 overexpression increased cgas ubiquitination but reduced its protein expression in comparison to the control group (Figure 4L). The type of cgas ubiquitination that Trim26 regulates was examined. The modulation of intracellular

protein levels has been connected to several polyubiquitination activities, such as the ubiquitination of lysine 6 (K6), K11, K27, K29, K33, K48, and K63 linked ubiquitin[23]. WT and K48-linked polyubiquitination of cgas were greatly increased by Trim26 overexpression but this effect was not shown in the other ubiquitination links in cgas (K6, K11, K27, K29, K33, or K63) (Figure 4M). The above data revealed that Trim26 specifically modifies the ubiquitination level of K48 polyubiquitin chains in cgas protein.

Trim26 is composed of four domains, including N-terminal RING domain, B-box domain, Coiled-coil domain and C-terminal B30.2/SPRY domain, each of which is crucial to its operation[24]. For instance, the Coiled-coil domain is involved in the formation of TRIM26 homodimers. Furthermore, Trim26 inhibited the interaction of SOX2 binding to WWP2 through the C-terminal domain, thereby regulating the progression of glioblastoma[25]. Through molecular docking studies, a series of mutants lacking specific domains of Trim26 and cgas were generated. This approach aimed to elucidate the interacting domains of both proteins, thereby offering valuable insights into the molecular mechanisms governing their relationship (Figures 5A, 5B, 5E). Our findings demonstrated that the interaction between Trim26 and cgas requires the B30.2/SPRY domain of Trim26 (Figures 5C,5D) and the C-terminal domain of cgas (Figures 5F). To further identify the ubiquitination site of cgas, we co-transfected cgas mutant with HAUb K48 and Myc-Trim26 into macrophages. The point mutant, K382R, exhibited a further reduction in ubiquitination. The results suggested that Trim26 mediates the K48-linked ubiquitination of cgas at K382 (Figures 5G). Additionally, point mutants of Trim26 were created in macrophages, showing that the C443A mutant of Trim26 in its B30.2/SPRY domain did not alter cgas ubiquitination. Moreover, this mutation did not influence the degradation of cgas subsequent to treatment with cycloheximide (CHX) (Figure 5H). Therefore, the ubiquitin-specific peptidase domain of Trim26, the B30.2/SPRY domain, is the primary regulator of interaction between Trim26 and cgas. BMDMs were co-transfected with Flag-cgas, HA-Ub, and Myc-

Trim26 (wild-type, WT) or Myc-C443A mutant (Figure 5I) to elucidate the regulatory function of Trim26-mediated cgas ubiquitination. Similarly, K48-linked ubiquitination was elevated by Trim26 overexpression, however, this shift was reversed by transfecting the C443A mutant plasmid (Figure 5J), suggesting that Trim26 interacts with cgas via ubiquitination to reduce cgas stability.

The melatonin/Nfatc1/Trim26 axis inhibits macrophages senescence through restricting cgas/ Sting signaling

Accumulating evidence suggests that cGAS/STING signaling not only activates innate immunity but also induces cellular senescence in a cell autonomous mode[26]. Since melatonin served a critical player responsible for the activation of the Nfatc1/Trim26/cgas axis, we further determined whether melatonin impacted the cgas/Sting pathway to defend macrophages against senescence. Upon Trim26 overexpression or cgas loss in BMDMs, along with melatonin stimulation, phosphorylation levels of Sting (p-Sting), Tbk1 (p-Tbk1) and Irf3 (p-Irf3) expression decreased without altering the total protein levels of Sting, Tbk1, and Irf3 (Figure 6A, 6B). Overexpression of cgas can effectively reverse the regulation of Trim26 on the expression of the above proteins (Figure 6C). Also, Trim26 loss elevated p-Sting, p-Tbk1, p-Irf3 and Il-6 production without changing Sting, Tbk1, and Irf3 protein levels. This effect was reversed by cgas overexpression but not by the Trim26 mutant (C443A) (Figure 6D-6F). Conversely, silencing Trim26 increased Il-6 expression, which could be rescued by cgas loss or sting loss (Figure 6G,6H). Subsequently, the role of cgas in enhancing tumor growth and influencing therapy sensitivity was evaluated in vivo. To assess tumor formation, 4T1 cells were co-injected into liposome-treated BALB/c mice along with BMDMs that had specific Trim26 alterations, with or without cgas overexpression. Once the tumors grew to a volume of 100 mm^3, the mice received weekly doxorubicin treatments at a dose of 5 mg/kg for four consecutive weeks (Figure 6I,6J). Immunofluorescence staining of tumor-bearing mice showed a marked increase

in $p16^+$ and $F4/80^+$expressing cells in both vector and Trim26+cgas overexpression groups compared to the Trim26 overexpression group (Figures 6K). There was also significantly higher SA-β-gal activity of BMDM cells in both vector and Trim26+cgas overexpression groups compared to the Trim26 overexpression group (49.7% or 47% versus 9.8%, respectively) ($P < 0.05$; Figure 6L). Moreover, greatly elevated expression of Il-6 was observed in the Trim26+cgas overexpression group (Figure 6M). Collectively, the melatonin/Nfatc1/Trim26 axis inhibited macrophages senescence and increased chemotherapy responsiveness through restricting cgas/ Sting signaling.

Cotreatment with melatonin and cgas inhibitor G150 act together to increase chemotherapy responsiveness

To further confirm the role of $cgas^{K382R}$ in the melatonin regulation of macrophages and its effect on tumor suppression, BMDMs from BALB/c mice underwent cgas knockdown followed by $cgas^{K382R}$ overexpression via lentiviral transduction. These modified BMDMs were then reintroduced into liposome-treated mice through tail vein infusion. Once the xenotransplanted tumors became palpable and reached a uniform volume of 100 mm^3, treatments were administered: either DMSO or melatonin, each combined with doxorubicin. Two additional groups of wild-type mice were treated with melatonin and cgas inhibitors (G150). The $cgas^{K382R}$ mutation diminished the ability of melatonin to boost the efficacy of breast cancer chemotherapy. Melatonin treatment in combination significantly hindered tumor growth in wild-type (WT) BALB/c mice compared to G150 treatment alone (Figure 7A,7B). Collectively, these findings indicate that melatonin modulates macrophage senescence through cgas ubiquitination, consequently influencing TNBC chemotherapy responsiveness. The proliferation, apoptotic indices and immunofluorescence staining of tumor tissue provided evidence that the $cgas^{K382R}$ mutation serves as a critical factor in mediating melatonin-induced inhibition of macrophage cellular senescence (Figure 7C-7E). ELISA assays and SA-β-gal also exhibited corresponding alterations as per these observations (Figure 7F,7G).

Taken together, our data provided proof-of-principle evidence that targeting melatonin/Nfatc1/Trim26 axis can supress macrophage senescence and overcome chemotherapy resistance through inhibiting cgas/Sting activation (Figure 7H). Also, the employment of melatonin and cgas inhibitor may provide viable strategy for future TNBC treatment.

Discussion

We have identified that reduced melatonin levels are associated with chemoresistance in mice and human. Upon examining the decline in mice, melatonin deficiency has been discovered leading to TAMs senescence and immune dysfunction. Macrophages, as versatile immune cells that respond to infection and maintain tissue homeostasis, are believed to play crucial but not entirely understood roles in monitoring and managing senescent cells[27, 28]. We found that in cases of chemotherapy with melatonin deficiency, macrophages undergo senescence and significantly lose immunosurveillance capacity. Macrophages lacking melatonin secrete large quantities of SASP-associated factors, which lead to tissue inflammation, immune system dysfunction, and chemoresistance. Despite ongoing debates regarding the senescence potential of macrophages, our data affirm that melatonin-deficient macrophages acquire senescence characteristics.

Chemoresistance is frequently associated with heightened cellular senescence within the tumor microenvironment. This senescence can arise following prior chemotherapy treatments across various solid tumors[29-31]. Melatonin, which is secreted in a rhythmic pattern by the mammalian pineal gland, plays a significant role in the regulation of aging, is known for its neuroprotective properties[32] and also acts as a highly effective scavenger of free radicals[33]. Melatonin safeguards neurons by mitigating the loss of mitochondrial membrane potential (MMP), preventing cytochrome c release, reducing caspase activation, decreasing reactive oxygen species (ROS) accumulation, and inhibiting the activation of proinflammatory cytokines during neurodegenerative processes[34, 35]. Melatonin levels decline steadily as individuals age, potentially leading

to increased cancer progression and immune system dysfunction, which are commonly observed in aging[36, 37]. Although there is evidence that melatonin is associated with the progression of breast cancer, its molecular mechanism of regulating TNBC remains to be further explored[38].

As immune cells residing in tumors, macrophages are exposed to diverse stressors that can induce cellular senescence. The innate immune response acts as the frontline defense against viruses and cancer. However, macrophages, akin to other cellular entities, are capable of entering a senescent state. Recent research has uncovered a distinct population of tissue-resident lung macrophages that indirectly promote lung tumor growth by fostering an immunosuppressive tumor microenvironment[39]. Eliminating senescent macrophages leads to the disruption of the vascular network within tumors, thereby diminishing both tumor proliferation and invasiveness[15]. This research illustrates that melatonin augments the efficacy of chemotherapy in TNBC and improves patient outcomes by suppressing macrophage senescence.

The cGAS-STING pathway is a critical immune defense mechanism against invasion by a wide range of pathogens[40]. As initial responders of the immune system, macrophages serve dual purposes: executing effector functions to combat pathogens and acting as sentinels to signal various threats to other immune cells, thus initiating and orchestrating a diverse immune response[41]. STING activation in macrophages resulted in the secretion of interleukin (IL-1β and IL-18) and enhancing the antitumor function of NK cells[42]. Hang Yin[43] discovered that the E3 ubiquitin ligase, MARCH8, acts to inhibit the signaling pathways driven by cGAS. The polyubiquitylation process reduced the DNA binding capacity of cGAS, diminished cGAMP synthesis, and weakened the subsequent innate immune response. In our study, RNA sequencing indicated that melatonin suppresses the expression of aging-related pathways downstream by upregulating Trim26 transcription in macrophages. It has been reported that cGAS localizes to the plasma membrane to halt abnormal IFN activity triggered by self-DNA[44]. Prior investigations revealed that cGAS activity is regulated by

monoubiquitylation, as well as ubiquitylation linked through K27, K48, and K63[43, 45-47]. As far as we know, the regulation of cGAS through ubiquitination in macrophages has not yet been documented. Here, we discovered K48-linked ubiquitination on cgas and then explored its functional implications. Through LC-MS/MS analysis and subsequent validation via ubiquitylation assay, we determined that Trim26 mediates K48-linked polyubiquitination at Lys382 of cgas. Further investigation into the mechanism revealed that the ubiquitin attached to Lys382 of cgas impedes its capacity to inhibit the cgas-Sing signaling cascade.

Our research demonstrated that the concomitant use of the cgas inhibitor PF-0692821 with melatonin markedly suppresses cellular proliferation and alleviates senescence in TAMs. These findings may provide a mechanistic insight into the enhanced anti-tumor efficacy observed in the combination treatment, thereby impeding the advancement of TNBC. To our understanding, this research represents the inaugural investigation into the functional role and underlying mechanisms by which melatonin may modulate chemoresistance in TNBC.

In summary, we uncovered a novel function of melatonin in modulating cgas-driven senescence signaling. Melatonin regulated Trim26, which consistently engages with cgas to promote its K48-linked polyubiquitination at Lys382, effectively blocking the cgas-Sing signaling pathway and curbing TAMs senescence. Our research reveals a link between K48-linked polyubiquitination of cgas and the control of macrophage aging. Given that cgas overactivation leads to TAMs senescence and chemoresistance, elucidating the mechanism by which melatonin suppresses cgas could reveal new therapeutic targets for addressing TNBC.

Experimental Procedures

Study patients

A total of 30 TNBC samples were obtained from the Breast Center of the First Affiliated Hospital of Nanjing Medical University. All patients received neoadjuvant

chemotherapy with taxane or anthracycline. The patients who had received immunotherapy were excluded. The response of patients to chemotherapy was evaluated based on postoperative pathology and divided into two groups: response (Res) and non-response (Non-res). Supplementary Table 1 displays the anonymised clinicopathological characteristic data. Every patient gave their informed permission, and our study was authorized by the ethics committee of the First Affiliated Hospital of Nanjing Medical University. Our research complied with the Declaration of Helsinki principles. This study was approved by the Ethics Committee of the First Affiliated Hospital of Nanjing Medical University (approval number: V20210119)

Cell lines and plasmids

Murine breast cancer cell line (4T1) and mouse macrophages cell lines (BMDM) were used in this study. BMDM were obtained as follows. After the mice were executed, their femurs and tibia bones were soaked in 75% ethanol. The connected muscle and adipose tissues were excised, and then cut off the two ends of bones. The bone marrow was washed with PBS extracted with a syringe to a 40μm filter. The flushing fluid was collected in centrifuge tube, centrifuged at 1200 Revolutions Per Minute (r), 5 minutes (min), discard the supernatant and the added 1ml ACK Lysis Buffer. After 2 minutes, centrifuged the centrifuge tube at 1200r, 5 min again and discard the supernatant. Cell precipitate resuspended by 20% DMEM containing L929 cell supernatant and cultured with 20 ng/ml recombinant mouse M-CSF. All the cells were cultured at 37°C under 5% CO_2.

Genebay Biotech provided the plasmids that code for K6-, K11-, K27-, K29-, K33-, K48- and K63- linked HA-tagged ubiquitin. Lentiviral constructs for Trim26 and cgas were constructed by Corues Biotechnology. Trim26 and cgas truncation mutants were produced in accordance with the manufacturer's instructions using a KOD-Plus-Mutagenesis kit (Toyota, Osaka, Japan). Transient transfections with shRNAs and plasmids were executed using Lipofectamine 2000 or 3000, supplied by Thermo Fisher

Scientific. The shRNA sequences utilized in this study are detailed in Supplementary Table 2, while the plasmid constructs employed are cataloged in Supplementary Table 3.

BMDM cells were transduced with lentiviruses encoding shRNAs, specifically shNC, shTrim26-1, shTrim26-2, and shTrim26-3. Additionally, various lentiviral constructs from OBiO Technology were utilized to infect cells for the purpose of ectopic expression and functional analysis. These constructs included full-length Trim26 (Myc-Trim26), as well as several domain-specific deletion mutants: a RING-finger domain deletion (Myc-Trim26 ΔRING), a B-box domain deletion (Myc-Trim26 ΔB-box), a Coiled-coil domain deletion (Myc-Trim26 ΔCoiled-coil), and a SPRY domain deletion (Myc-Trim26 ΔB30.2/SPRY). Furthermore, cells were also infected with constructs harboring point mutations: C53,56A, C359A, and C443A mutations in Trim26, and K382R, K472R mutations in cgas.

Mice model assay

BALB/c mice (five-week-old, female) were given an injection of $5*10^4$/50 μl 4T1 cells via the nipple region into the mammary fat pad. When tumors grew to a volume of 100 mm^3, we randomly divided the mice into two groups and each were intraperitoneally injected with 10 mg/kg/d melatonin or DMSO as control every three days. Meanwhile, doxorubicin (5 mg/kg per week) was injected intraperitoneally for four weeks.

For the role of Trim26 and cgas investigations, a total of $5*10^4$/50 μl 4T1 cells were injected into the mammary fat pad of BALB/c mice on the day 0 of experiment. The BALB/c mice was injected intravenously with clodronate liposome (200 μl per mouse, FormuMax Scientific, F70101C-N) one day before tumor cell implantation and every 4 days thereafter. On the day 1 of experiment, $1*10^6$/50 μl BMDM-shTrim26, Trim26 or Trim26+cgas and control (BMDM-shNC or Vector) were injected intravenously into 4T1 cell-challenged host BALB/c mice respectively. The mice then received macrophage adoptive transfer treatment every 6 days, using the same methodology as

the first treatment. When tumors grew to a volume of 100 mm^3, BALB/c mice were intraperitoneally injected with 10 mg/kg/d melatonin or DMSO as control every three days, and doxorubicin (5 mg/kg per week) for four weeks.

To evaluate the clinical translational value, we initially achieved the knockdown of cgas in BMDM cells. Then cgas WT or K472R mutants were re-introduced into cgas-knockdown BMDMs. The procedure of macrophages clearance and transfusion, TNBC model construction and chemotherapy administration in mice was similar to before. When tumours grew to a volume of 100 mm^3, the BALB/c mice were treated with melatonin or DMSO or cgas inhibitors (10mg/kg, i.p., qod) or the combination of melatonin and cgas inhibitors, while each group received 4 weeks of chemotherapy. Dimethyl sulfoxide (DMSO) was used to dissolve the melatonin (HY-B0075, MCE) to create a 1 M solution, which was then kept at -20°C. G150 (HY-128583, MCE) was used as cGAS inhibitors. Doxorubicin (HY-15142A, MCE), Luzindole (117946-91-5, Sigma), 4-P-PDOT (134865-74-0, Sigma) were applied in this assay. All mice were euthanized after 4 weeks of DOX treatment via cervical dislocation. Animal experiment is ethically acceptable as 2310107.

Measurement of plasma metabolism

The levels of senescence-associated metabolism including γ-aminobutyric acid (GABA), dopamine, melatonin, β-nicotinamide mononucleotide (NMN) and α-Ketoglutarate (α-KG) in patients' serum were detected by using ELISA method. The kits we used were listed as follows: Human GABA Elisa Kit (B160295, Shanghai Hengyuan biological), DA(Dopamine) ELISA Kit (E-EL-0046, Elabscience), Human MT(Melatonin) ELISA Kit (E-EL-H2016, Elabscience), NMN elisa kit (HBP37953R, ShanghaiHuabang biological), α-Ketoglutarate (α-KG) Fluorometric Assay Kit (E-BC-F047, Elabscience).

Multiplex immunofluorescence staining and confocal microscopy

Paraffin sections of tumor tissues were prepared. Multi-color immunofluorescence assays were performed following the procedure provided by a Five-colour Fluorescence kit (Recordbio Biological Technology, RC0086-45RM). Antibodies for multi-color immunofluorescence were: F4/80 (ab300421, Abcam), CD68 (ab303565, Abcam), p16 (10883-1-AP, Proteintech).

BMDMs were frozen for 15 minutes with 4% paraformaldehyde. After that, they were cultured for 30 minutes with 0.5% Triton-X and blocked for 30 minutes with 5% BSA. Primary antibody diluent was employed, and the mixture was incubated for the whole night at 4 °C. DAPI was used to label the cell nuclei. Photographs of colocalization were acquired with a confocal microscope (Leica DMI3000 B).

SA-β-gal staining

Senescence β-Galactosidase Staining Kit (Beyotime, C0602) was used to perform SA-β-gal staining in accordance with the manufacturer's instructions. Briefly, three biological replicates of each group cells were fixed for five minutes at room temperature using 2% formaldehyde and 0.2% glutaraldehyde and followed by PBS washing. The staining solution then incubated the cells overnight at 37 °C. The ImageJ software was used for the measurement of SA-β-gal-positive cells.

ELISA

The ELISA was carried out in accordance with the manufacturer's recommendations. cells were planted into a 96-well plate at the proper concentration and cultivated for 24 hours. After that, serum-free DMEM was added in an equal amount to replace the cell culture medium. After 24 hours, the supernatants were collected, and any floating cells were filtered out using a 0.45 mm filter. Il-6 (E-EL-M0044), Il-1α (E-EL-M3059), Tnf-α (E-EL-M3063), Mmp3 (E-EL-M0626), Igfbp2 (E-EL-M3086) were purchased from Elabscience.

Extracellular acidification and oxygen consumption rate

A Seahorse Bioscience instrument (XF24, Agilent) and a Seahorse Bioscience instrument (XF96 Agilent) was used to measure OCR and ECAR. Following was the chemical concentration used: Glucose (10 mM), Oligomycin A (1.5 μM), 2-deoxy-glucose (2DG) (50 mM), Carbonyl cyanide 4-(trifluoromethoxy) phenylhydrazone (FCC) (2.0 μM), and a combination of rotenone (500 nM) and antimycin A (500 nM). Specific steps were followed according to the manufacturer's guidelines.

CHIP assays

BMDMs transfected with shNC/shNfarc1 underwent a 10-minute cross-linking process using 1% formaldehyde at room temperature. The specific steps referred to the guidelines of EZ CHIP KIT 22 ASSAYS (MILLIPORE; 17-371). Quantitative reverse transcription polymerase chain reaction (qRT-PCR) was used to evaluate changes in Nfarc1accumulation at the Trim26 promoter region. ΔCt [normalized ChIP] = Ct [ChIP] - (Ct [Input] -Log2 (Factor of Input Dilution)); Factor of Input Dilution = (fraction of the input chromatin saved) -1. %Input = 2(-ΔCt [normalized ChIP]) *100%. In Supplementary Table 4, the primers that were utilized are provided.

RNA extraction and qRT-PCR assays

Total RNA was extracted from cells and tissues using RNA Extraction Kit (Vazyme). The cDNA was synthesized by using reverse transcription system (Toyobo). qRT-PCR was then carried out using SYBR Green PCR Master Mix. Three duplicates of each sample were tested. In Supplementary Table 5, the primers that were utilized are provided.

Western blot assay

Cells and breast cancer tissues were lysed by Radioimmunoprecipitation assay (RIPA) Lysis Buffer (Beyotime). SDS-PAGE was used to separate equivalent quantities of

protein, which was then transferred to a membrane, treated with different primary and secondary antibodies. The data were collected using Image J software.

Immunoprecipitation coupled with mass spectrometry (IP/MS)

Total proteins were isolated from BMDMs and immunoprecipitated by utilizing suitable primary antibody and protein A/G-agarose beads (Beyotime). After that, the immunoprecipitations were extracted and analyzed using mass spectrometry.

Deubiquitination assay

In order to conduct the in vivo ubiquitination test, the specified plasmids were co-transfected into BMDMs. Ubiquitin antibody immunoblotting is then used to measure endogenous cgas ubiquitination.

Following the manufacturer's suggested procedure, in vitro ubiquitination was examined using a ubiquitination kit (Boston Biochem, USA). In a nutshell, Flag-cgas and Myc-Trim26 proteins were produced in vitro, treated with ubiquitin conjugation mixture and then the ubiquitination of the cgas protein was determined using a CO-IP test.

GST pull-down assay

Pure GST- Trim26 protein was isolated from E. coli BL21 and treated with GST-cgas proteins. To thoroughly separate the GST proteins, Protein G beads were utilized. Finally, using immunoblotting, the bound forms of Trim26 and cgas were identified.

Immunoprecipitation (IP)

BMDMs were lysed in RIPA lysis solution (Thermo Fisher Scientific). Twenty L of protein A/G-agarose beads (Thermo Fisher Scientific) were added after 200 of total cellular proteins treated with antibodies for an overnight period at 4 °C. The precipitates

were boiled in SDS sample buffer after being rinsed four times with lysis buffer. With the proper antibodies, immunoblotting was performed on the supernatant.

TUNEL assay

The TUNEL assay was conducted using the In Situ Cell Death Detection Kit (Servicebio, China). Follow the specific steps according to the instructions. The following equation was used to calculate the apoptotic index of the cancer cells: apoptotic cells/total cells 100%.

Statistics analysis

R software (version 4.0.1) and GraphPad Prism version 8 (GraphPad Software) were both used for all statistical analyses. Bar graphs were displayed as mean ± SD values. To compare two groups impacted by a single variable, a two-sided Student's t test was employed. To compare different data groups impacted by one or two distinct variables respectively, one-way ANOVA or two-way ANOVA with Turkey's test were utilized. The Kaplan-Meier technique was used to create the survival curves, and the log-rank t-test was used to evaluate the data. ns, not significant; *$p<0.05$, **$p<0.01$, ***$p<0.001$.

Declaration

Ethics approval and consent to participate

This study was approved by the Ethics Committee of the First Affiliated Hospital of Nanjing Medical University (approval number: V20210119). Animal experiment is ethically acceptable as 2310107. The whole experimental protocols performed were approved by the Institutional Animal Care and Use Committee of Nanjing Medical University and in strict compliance with NIH Guide for the Care and Use of Laboratory Animals.

Consent for publication

Not applicable.

Data availability

The datasets supporting the conclusions of this article are included within the article and its additional files.

Competing interest

None

Funding

The current study was funded by the National Natural Science Foundation of China (Grant Nos. 82403355) and China Postdoctoral Science Foundation (2024M763329).

Authors' contributions

XZ, MZ and HZ performed all the experiments, prepared the figures, and drafted the manuscript. JY and XW revised the manuscript. XL, JT, XY and YZ took part in the study management, provided guidance. All authors reviewed and authorized the final version.

Acknowledgements

Not applicable.

References

1. Siegel RL, Giaquinto AN, Jemal A. **Cancer statistics, 2024**. *CA Cancer J Clin* 2024; 74(1):12-49.
2. Sorlie T, Perou CM, Tibshirani R, Aas T, Geisler S, Johnsen H, et al. **Gene expression patterns of breast carcinomas distinguish tumor subclasses with clinical implications**. *Proc Natl Acad Sci U S A* 2001; 98(19):10869-10874.
3. Bianchini G, De Angelis C, Licata L, Gianni L. **Treatment landscape of triple-negative breast cancer - expanded options, evolving needs**. *Nat Rev Clin Oncol* 2022; 19(2):91-113.

4. Liu B, Liu X, Han L, Chen X, Wu X, Wu J, et al. **BRD4-directed super-enhancer organization of transcription repression programs links to chemotherapeutic efficacy in breast cancer**. *Proc Natl Acad Sci U S A* 2022; 119(6).
5. Gorgoulis V, Adams PD, Alimonti A, Bennett DC, Bischof O, Bishop C, et al. **Cellular Senescence: Defining a Path Forward**. *Cell* 2019; 179(4):813-827.
6. Lopez-Otin C, Blasco MA, Partridge L, Serrano M, Kroemer G. **Hallmarks of aging: An expanding universe**. *Cell* 2023; 186(2):243-278.
7. Herranz N, Gil J. **Mechanisms and functions of cellular senescence**. *J Clin Invest* 2018; 128(4):1238-1246.
8. Victorelli S, Salmonowicz H, Chapman J, Martini H, Vizioli MG, Riley JS, et al. **Apoptotic stress causes mtDNA release during senescence and drives the SASP**. *Nature* 2023; 622(7983):627-636.
9. Sturmlechner I, Zhang C, Sine CC, van Deursen EJ, Jeganathan KB, Hamada N, et al. **p21 produces a bioactive secretome that places stressed cells under immunosurveillance**. *Science* 2021; 374(6567):eabb3420.
10. Krizhanovsky V, Yon M, Dickins RA, Hearn S, Simon J, Miething C, et al. **Senescence of activated stellate cells limits liver fibrosis**. *Cell* 2008; 134(4):657-667.
11. Brigger D, Riether C, van Brummelen R, Mosher KI, Shiu A, Ding Z, et al. **Eosinophils regulate adipose tissue inflammation and sustain physical and immunological fitness in old age**. *Nat Metab* 2020; 2(8):688-702.
12. Krishnarajah S, Ingelfinger F, Friebel E, Cansever D, Amorim A, Andreadou M, et al. **Single-cell profiling of immune system alterations in lymphoid, barrier and solid tissues in aged mice**. *Nat Aging* 2022; 2(1):74-89.
13. Yousefzadeh MJ, Flores RR, Zhu Y, Schmiechen ZC, Brooks RW, Trussoni CE, et al. **An aged immune system drives senescence and ageing of solid organs**. *Nature* 2021; 594(7861):100-105.
14. Moiseeva V, Cisneros A, Sica V, Deryagin O, Lai Y, Jung S, et al. **Senescence atlas reveals an aged-like inflamed niche that blunts muscle regeneration**. *Nature* 2023; 613(7942):169-178.
15. Haston S, Gonzalez-Gualda E, Morsli S, Ge J, Reen V, Calderwood A, et al. **Clearance of senescent macrophages ameliorates tumorigenesis in KRAS-driven lung cancer**. *Cancer Cell* 2023; 41(7):1242-1260 e1246.
16. Schmitt CA, Wang B, Demaria M. **Senescence and cancer - role and therapeutic opportunities**. *Nat Rev Clin Oncol* 2022; 19(10):619-636.
17. Prieto LI, Sturmlechner I, Graves SI, Zhang C, Goplen NP, Yi ES, et al. **Senescent alveolar macrophages promote early-stage lung tumorigenesis**. *Cancer Cell* 2023; 41(7):1261-1275 e1266.
18. Gasek NS, Kuchel GA, Kirkland JL, Xu M. **Strategies for Targeting Senescent Cells in Human Disease**. *Nat Aging* 2021; 1(10):870-879.
19. Arner EN, Rathmell JC. **Metabolic programming and immune suppression in the tumor microenvironment**. *Cancer Cell* 2023; 41(3):421-433.

20. Johansson LC, Stauch B, McCorvy JD, Han GW, Patel N, Huang XP, et al. **XFEL structures of the human MT(2) melatonin receptor reveal the basis of subtype selectivity**. *Nature* 2019; 569(7755):289-292.
21. Li X, Yuan J, Song C, Lei Y, Xu J, Zhang G, et al. **Deubiquitinase USP39 and E3 ligase TRIM26 balance the level of ZEB1 ubiquitination and thereby determine the progression of hepatocellular carcinoma**. *Cell Death Differ* 2021; 28(8):2315-2332.
22. Wang Z, Xia Y, Wang Y, Zhu R, Li H, Liu Y, et al. **The E3 ligase TRIM26 suppresses ferroptosis through catalyzing K63-linked ubiquitination of GPX4 in glioma**. *Cell Death Dis* 2023; 14(10):695.
23. Michel MA, Elliott PR, Swatek KN, Simicek M, Pruneda JN, Wagstaff JL, et al. **Assembly and specific recognition of k29- and k33-linked polyubiquitin**. *Mol Cell* 2015; 58(1):95-109.
24. Xu M, Tan J, Liu X, Han L, Ge C, Zhang Y, et al. **Tripartite motif containing 26 prevents steatohepatitis progression by suppressing C/EBPdelta signalling activation**. *Nat Commun* 2023; 14(1):6384.
25. Mahlokozera T, Patel B, Chen H, Desouza P, Qu X, Mao DD, et al. **Competitive binding of E3 ligases TRIM26 and WWP2 controls SOX2 in glioblastoma**. *Nat Commun* 2021; 12(1):6321.
26. Chen C, Xu P. **Cellular functions of cGAS-STING signaling**. *Trends Cell Biol* 2023; 33(8):630-648.
27. Mass E, Nimmerjahn F, Kierdorf K, Schlitzer A. **Tissue-specific macrophages: how they develop and choreograph tissue biology**. *Nat Rev Immunol* 2023; 23(9):563-579.
28. Guilliams M, Thierry GR, Bonnardel J, Bajenoff M. **Establishment and Maintenance of the Macrophage Niche**. *Immunity* 2020; 52(3):434-451.
29. Zander SA, Kersbergen A, van der Burg E, de Water N, van Tellingen O, Gunnarsdottir S, et al. **Sensitivity and acquired resistance of BRCA1;p53-deficient mouse mammary tumors to the topoisomerase I inhibitor topotecan**. *Cancer Res* 2010; 70(4):1700-1710.
30. Rottenberg S, Nygren AO, Pajic M, van Leeuwen FW, van der Heijden I, van de Wetering K, et al. **Selective induction of chemotherapy resistance of mammary tumors in a conditional mouse model for hereditary breast cancer**. *Proc Natl Acad Sci U S A* 2007; 104(29):12117-12122.
31. Fan G, Yu B, Tang L, Zhu R, Chen J, Zhu Y, et al. **TSPAN8(+) myofibroblastic cancer-associated fibroblasts promote chemoresistance in patients with breast cancer**. *Sci Transl Med* 2024; 16(741):eadj5705.
32. Wang X, Sirianni A, Pei Z, Cormier K, Smith K, Jiang J, et al. **The melatonin MT1 receptor axis modulates mutant Huntingtin-mediated toxicity**. *J Neurosci* 2011; 31(41):14496-14507.

33. Wakatsuki A, Okatani Y, Izumiya C, Ikenoue N. **Melatonin protects against ischemia and reperfusion-induced oxidative lipid and DNA damage in fetal rat brain**. *J Pineal Res* 1999; 26(3):147-152.
34. Zhang HM, Zhang Y. **Melatonin: a well-documented antioxidant with conditional pro-oxidant actions**. *J Pineal Res* 2014; 57(2):131-146.
35. Esposito E, Cuzzocrea S. **Antiinflammatory activity of melatonin in central nervous system**. *Curr Neuropharmacol* 2010; 8(3):228-242.
36. Jauhari A, Baranov SV, Suofu Y, Kim J, Singh T, Yablonska S, et al. **Melatonin inhibits cytosolic mitochondrial DNA-induced neuroinflammatory signaling in accelerated aging and neurodegeneration**. *J Clin Invest* 2020; 130(6):3124-3136.
37. Shi YS, Yang TN, Wang YX, Ma XY, Liu S, Zhao Y, et al. **Melatonin Mitigates Atrazine-Induced Renal Tubular Epithelial Cell Senescence by Promoting Parkin-Mediated Mitophagy**. *Research (Wash D C)* 2024; 7:0378.
38. Yang A, Peng F, Zhu L, Li X, Ou S, Huang Z, et al. **Melatonin inhibits triple-negative breast cancer progression through the Lnc049808-FUNDC1 pathway**. *Cell Death Dis* 2021; 12(8):712.
39. Casanova-Acebes M, Dalla E, Leader AM, LeBerichel J, Nikolic J, Morales BM, et al. **Tissue-resident macrophages provide a pro-tumorigenic niche to early NSCLC cells**. *Nature* 2021; 595(7868):578-584.
40. Tan X, Sun L, Chen J, Chen ZJ. **Detection of Microbial Infections Through Innate Immune Sensing of Nucleic Acids**. *Annu Rev Microbiol* 2018; 72:447-478.
41. Sheu KM, Hoffmann A. **Functional Hallmarks of Healthy Macrophage Responses: Their Regulatory Basis and Disease Relevance**. *Annu Rev Immunol* 2022; 40:295-321.
42. Sun Y, Hu H, Liu Z, Xu J, Gao Y, Zhan X, et al. **Macrophage STING signaling promotes NK cell to suppress colorectal cancer liver metastasis via 4-1BBL/4-1BB co-stimulation**. *J Immunother Cancer* 2023; 11(3).
43. Yang X, Shi C, Li H, Shen S, Su C, Yin H. **MARCH8 attenuates cGAS-mediated innate immune responses through ubiquitylation**. *Sci Signal* 2022; 15(732):eabk3067.
44. Barnett KC, Coronas-Serna JM, Zhou W, Ernandes MJ, Cao A, Kranzusch PJ, et al. **Phosphoinositide Interactions Position cGAS at the Plasma Membrane to Ensure Efficient Distinction between Self- and Viral DNA**. *Cell* 2019; 176(6):1432-1446 e1411.
45. Chen M, Meng Q, Qin Y, Liang P, Tan P, He L, et al. **TRIM14 Inhibits cGAS Degradation Mediated by Selective Autophagy Receptor p62 to Promote Innate Immune Responses**. *Mol Cell* 2016; 64(1):105-119.
46. Wang Q, Huang L, Hong Z, Lv Z, Mao Z, Tang Y, et al. **The E3 ubiquitin ligase RNF185 facilitates the cGAS-mediated innate immune response**. *PLoS Pathog* 2017; 13(3):e1006264.

47. Seo GJ, Kim C, Shin WJ, Sklan EH, Eoh H, Jung JU. **TRIM56-mediated monoubiquitination of cGAS for cytosolic DNA sensing**. *Nat Commun* 2018; 9(1):613.

818 **Figure legends**

819 FIGURE 1 | **Senescent macrophages are correlated with chemoresistance and**
820 **adverse prognosis**

821 A. A total of 13 distinct cell types were identified and visualized using UMAP. Each
822 cell type was distinguished by a unique color, integrating data from two individual
823 patients. B. The bar plot depicts the frequency distribution of each cell cluster. C.
824 KEGG pathway analysis performed on macrophage subsets to identify related enriched
825 pathways. D. Violin plot illustrates the distinct subclusters of cells and the expression
826 levels of cell senescence-associated genes. E, F. UMAP plot and violin plot showing
827 macrophage cell subcluster and senescence genes from both patients. G. Multicolour
828 Immunofluorescent using CD68 and p16 antibodies in patient tumour sections (n=15
829 pairs). Scale bar = 50 μm. H. Risk factors associated with unfavourable prognosis in
830 BC patients were evaluated by multivariate cox regression analysis. The data was based
831 on TCGA database. (n=166) I. Aging-related metabolites were measured by ELISA in
832 the peripheral blood of patients. (n=30) J. Melatonin levels in tumor-associated
833 macrophages (TAMs) were analysed by ELISA. (n=30) K. Scatter-plot showing
834 correlation between p16 staining intensity and expression levels of melatonin in
835 macrophages. A representative data set is displayed as mean ± SEM values. ns., not
836 significant, *$p < 0.05$, **$p < 0.01$, ***$p < 0.001$.

837

838 FIGURE 2 | **Melatonin improves chemotherapy responsiveness through inhibiting**
839 **macrophage senescence**

840 A. Schematic diagram showing cell culture system in vitro. BMDMs isolated from
841 BALB/c mice was pretreated with melatonin (0/10/50/100μM) for 48h and exposed to
842 1 μM doxorubicin (DOX) for 24 hours. B. The proportion of SA-β-gal$^+$ cells in BMDMs
843 after different concentrations of melatonin treatment. (n =5) C. The mRNA expression
844 of Il-6 and p21 was analysed by qRT-PCR in BMDMs, which were treated with
845 different concentrations of melatonin treatment. (n =5) D. qRT-PCR was performed to

846 determine the expression of senescence related factors, including Il-1α and p53 in
847 BMDMs. (n = 3) E. Western blot of senescence markers in macrophages. (n = 3) F. The
848 effects of melatonin on OCR and ECAR measurement in BMDMs. (G, H. DMSO or
849 luzindole or 4-P-PDOT was added at one hour prior to melatonin treatment. The rest
850 treatment of BMDMs was as same as above.) G, H. Representative images and
851 quantitative statistics of the SA-β-gal activity in different treatment groups (scale bar =
852 100μm). (n = 3) I. Secreted II-6, Il-1α, Mmp3, Tnf-α, and Igfbt2 amounts were analysed
853 by ELISA. J. The workflow of the drug administration procedure for the mouse
854 tumorigenicity model. K. Tumours were collected and photographed (n = 5), and
855 tumour volumes were measured. L. Tumour sections were stained with TUNEL (scale
856 bar = 25μm) and Ki67 IHC (scale bar = 200μm). M. Immunofluorescent images of
857 mouse tumour sections using F4/80 and p16 antibodies. Scale bar = 50 μm. A
858 representative data set is displayed as mean ± SEM values of three to five independent
859 biological replicates. ns., not significant, *p < 0.05, **p < 0.01, ***p < 0.001.
860
861 FIGURE 3 | **Melatonin inhibits macrophage senescence by boosting the**
862 **transcription of Trim26 through the induction of Nfatc1 in macrophages**
863 A. Volcano plot representing RNAseq analysis of differentially expressed genes
864 between melatonin group compared with DMSO group TAMs ($p \leq 0.05$; fold change $\geq$
865 0.5) B. GSEA ridge plots showed the significant representative pathways in melatonin
866 group. C. GSEA graphs from RNAseq data in melatonin group compared with DMSO
867 group TAMs. (A-C. n= 3 pairs) D. qRT-PCR was performed to assess Trim26 level in
868 DMSO and melatonin group. E. qRT-PCR was performed to determine the expression
869 of senescence related factors, including Il-6, Il-1α, p21, and p53 in BMDMs. F.
870 Representative images and quantitative statistics of the SA-β-gal activity in different
871 treatment groups (scale bar = 100μm). G, H. Tumours were collected and photographed
872 (n = 6), and tumour volumes were measured. I. Tumour sections were stained with
873 TUNEL (scale bar = 25μm) and Ki67 IHC (scale bar = 200μm). J. Immunofluorescent

images of mouse tumour sections using F4/80 and p16 antibodies. Scale bar = 50 μm. K. Relative luciferase activity of luciferase reporter plasmid containing Trim26 promoter in BMDMs transfected with plasmids overexpressing the five potential transcription factors or the control plasmid, combined with melatonin treatment for 48h. L. Relative mRNA levels of Trim26 in BMDMs transfected with indicated plasmids, combined with melatonin treatment for 48h. M. Relative mRNA levels of Trim26 in Nfatc1- or Vector-infected BMDMs, combined with melatonin treatment for 48h. N. Putative Nfatc1-binding sites within the genomic sequence that adjacent to the transcription start site of the Trim26 gene. O. Luciferase activities of Trim26 promoter reporter vectors in BMDMs. Red characters within the binding regions indicate putative or mutated Nfatc1 binding sequences. P. ChIP analysis of Nfatc1 binding to the Trim26 promoter in BMDMs. Q. BMDMs were treated with 50μM melatonin for 48h. Immunoblotting of Nfatc1. R. The localization of Nfatc1 with the treatment of DMSO or melatonin (scale bar = 10μm). S. BMDMs were transfected with Nfatc1. The cell lysates were then incubated with biotin-labeled melatonin and pulled down with streptavidin beads. The samples were immunoblotted with anti-Flag mAb. A representative data set is displayed as mean ± SEM values of three to six independent biological replicates. ns., not significant, *p < 0.05, **p < 0.01, ***p < 0.001.

FIGURE 4 | **Trim26 interacts with and degrades cgas**

A. Trim26-related protein analysis using coimmunoprecipitation and Coomassie brilliant blue staining in BMDM cells. B. Co-IP assays showed the binding of Trim26 with cgas. C, D. Exogenous protein interactions were verified in BMDMs. Lysates from BMDM cells transfected with Flag-tagged cgas and Myc-tagged Trim26 plasmids were immunoprecipitated with anti-Myc or anti-Flga, respectively. E. A GST pull-down assay was used to evaluate the direct interaction between Trim26 and cgas. F. Co-localization of Trim26 proteins (GREEN) with cgas proteins (RED) in BMDMs. Scale bar = 25 μm. G. Changes in endogenous cgas expression following

shTrim26 transfection. H, I. Trim26 and cgas protein levels were analysed by western blot in BMDM cells transfected with Trim26 (using proteasome inhibitor MG132 or lysosome inhibitors chloroquine (CQ)). J. cgas mRNA level in BMDM cells transfected with Vector and Trim26. K. The cgas protein level in designated timepoint after treatment with cycloheximide (CHX, 10 μg/ ml) in transfected BMDMs. L. cgas was pulled down and an anti-HA antibody was used to evaluated the ubiquitination levels of cgas. M. BMDMs were co-transfected with Flag-cgas and the indicated HA-Ub, K6-, K11-, K27-, K29-, K33-, K48-, or K63-linked-Ub, as well as the expression vector of Myc-Trim26 or the empty vector, and then the cgas ubiquitylation linkage was assessed. A representative data set is displayed as mean ± SEM values of three independent biological replicates. ns., not significant, *$p < 0.05$, **$p < 0.01$, ***$p < 0.001$.

FIGURE 5 | **Trim26 interacts with and degrades cgas**

A. A 3D structures was used to predict the specific binding sites for the interaction between Trim26 and cgas. B. Schematic illustration of Trim26, displaying the wild-type and truncations of Trim26. C. Co-IP analysis was used to assess the interaction between cgas and Trim26 or Trim26 truncation mutants in BMDM cells co-transfected with Myc-Trim26 plasmid or Myc-Trim26 truncation mutant plasmids together with Flag-cgas plasmid. D. Co-IP study of ubiquitination of cgas in BMDMs co-transfected with Myc-Trim26 or Myc-Trim26 truncations as well as HA-UB plasmid. E. Schematic illustration of cgas, displaying the wild-type and truncations of cgas. F. Co-IP analysis was used to assess the interaction between Trim26 and cgas or cgas truncation mutants in BMDM cells co-transfected with Flag-cgas plasmid or Flag-cgas truncation mutant plasmids together with Myc-Trim26 plasmid. G. cgas immunoprecipitation and western blotting with anti-Flag and anti-HA antibodies were used to assess cgas ubiquitination. H. Trim26 and its point mutations shown schematically. The binding cgas was identified by immunoprecipitating Trim26 and

its point mutations. The effects of Trim26 and its point mutations on cgas ubiquitination were verified. cgas and Trim26 protein levels were detected. For each of the three separate biological replicates, the data are shown as mean ± SEM. I. After transfecting BMDM cells with Myc-tagged Trim26 (WT) or Myc-tagged Trim26 (C443A), the lysates were immunoprecipitated with anti-Flag, followed by immunoblotting with anti-HA, anti-Myc, and anti-Flag. J. BMDMs were transfected with a plasmid expressing Flag-cgas, Myc-tagged Trim26 (WT and C443A), and K48-linked-Ub. Following a 3-hour exposure to MG132 (10 uM), the protein was extracted, immunoprecipitated using anti-Flag and immunoblotted using anti-HA, anti-Myc, and anti-Flag. A representative data set is displayed as mean ± SEM values of three independent biological replicates. ns., not significant, *$p < 0.05$, **$p < 0.01$, ***$p < 0.001$.

FIGURE 6 | **The melatonin/Nfatc1/Trim26 axis inhibits macrophages senescence through restricting cgas/ Sting signaling**

A. Immunoblotting in Trim26 overexpression BMDM cells melatonin starved and restored with melatonin (50 uM). B. Immunoblotting in cgas knockdown BMDM cells melatonin starved and restored with melatonin (50 uM). C. Immunoblotting in BMDM cells with concurrent Trim26 and cgas overexpression. D. Immunoblotting in Trim26 knockdown BMDM cells restored with or without cgas. E. qRT-PCR analysis in Trim26 knockdown BMDM restored with Trim26-WT or Trim26-C443A, Nfatc1 knockdown, melatonin starved and restored with melatonin (50 uM). F. Immunoblotting in Trim26 knockdown BMDM restored with Trim26-WT or Trim26-C443A, Nfatc1 knockdown. G. qRT-PCR analysis in Trim26 knockdown BMDM cells restored with or without cgas knockdown. H. qRT-PCR analysis in shNC, shTrim26, shTrim26+shcgas, and shTrim26+shSting BMDM cells. (A-H. n = 3 biological replicates) I. The workflow of the mouse tumorigenicity model. J. Tumors were collected and photographed (n = 6), and tumor volumes were measured. K.

Immunofluorescent images of mouse tumor sections using F4/80 and p16 antibodies. Scale bar = 50 μm. L. The proportion of SA-β-gal$^+$ cells in BMDMs with concurrent Trim26 and cgas overexpression. Scale bar = 100 μm. M. Secreted II-6 amounts were analysed by ELISA. A representative data set is displayed as mean ± SEM values of three to six independent biological replicates. ns., not significant, *p < 0.05, **p < 0.01, ***p < 0.001.

FIGURE 7 | **Cotreatment with melatonin and cgas inhibitor G150 act together to increase chemotherapy responsiveness**

A, B. Tumors were collected and photographed (n = 6), and tumor volumes were measured. C-E. TUNEL (scale bar = 25μm), Ki67 IHC (scale bar = 200μm) and immunofluorescent staining for F4/80 and p16 (scale bar = 50μm) in mouse tumor sections. F. Secreted II-6, Il-1α, Mmp3, and Tnf-α amounts were analysed by ELISA. G. Representative images and quantitative statistics of the SA-β-gal activity in different treatment groups (scale bar = 100μm). H. Illustration depicting the melatonin/Nfatc1/Trim26/cgas/Sting improves chemotherapy responsiveness through inhibiting macrophage senescence. A representative data set is displayed as mean ± SEM values of three to six independent biological replicates. ns., not significant, *p < 0.05, **p < 0.01, ***p < 0.001.

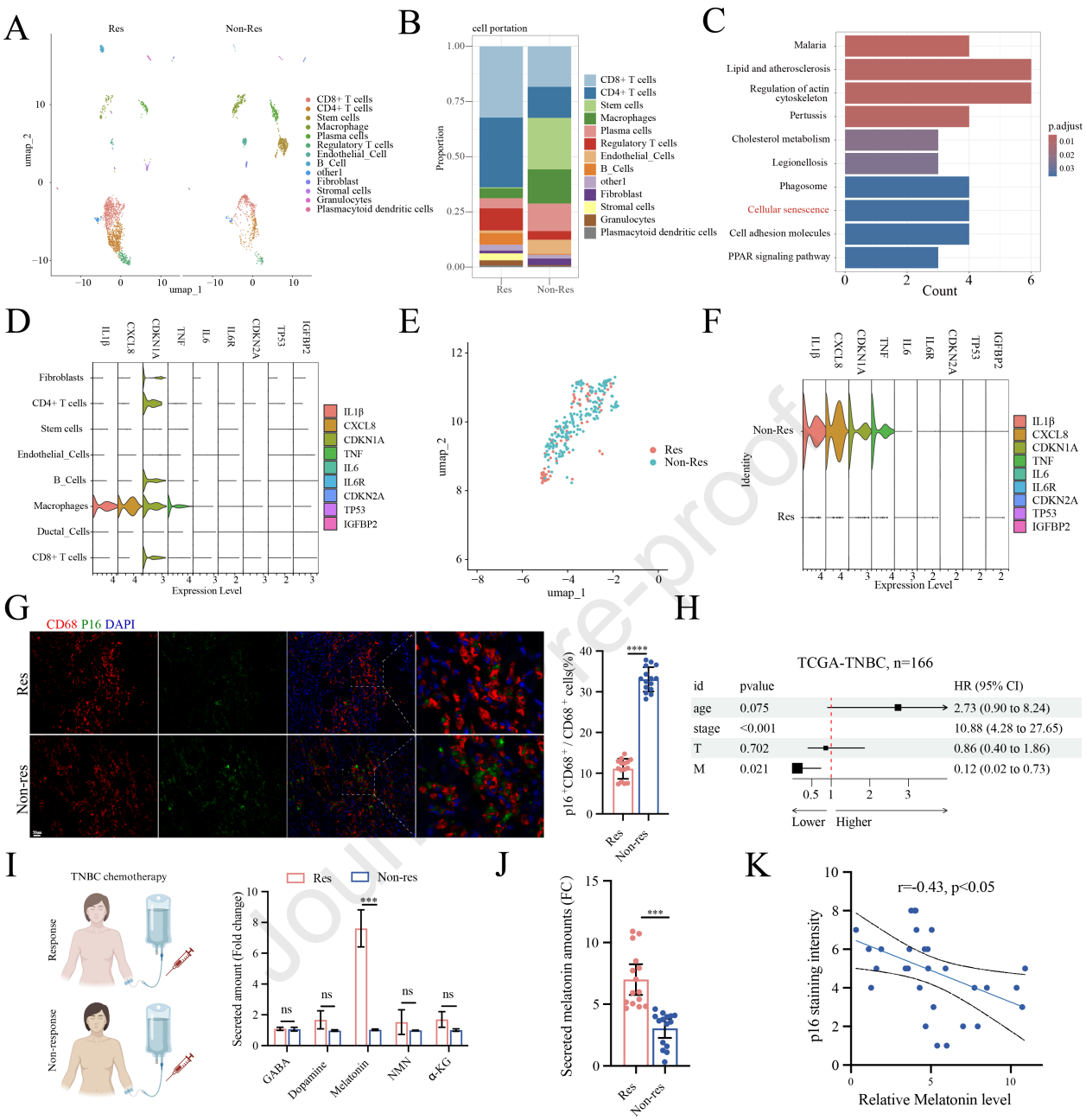

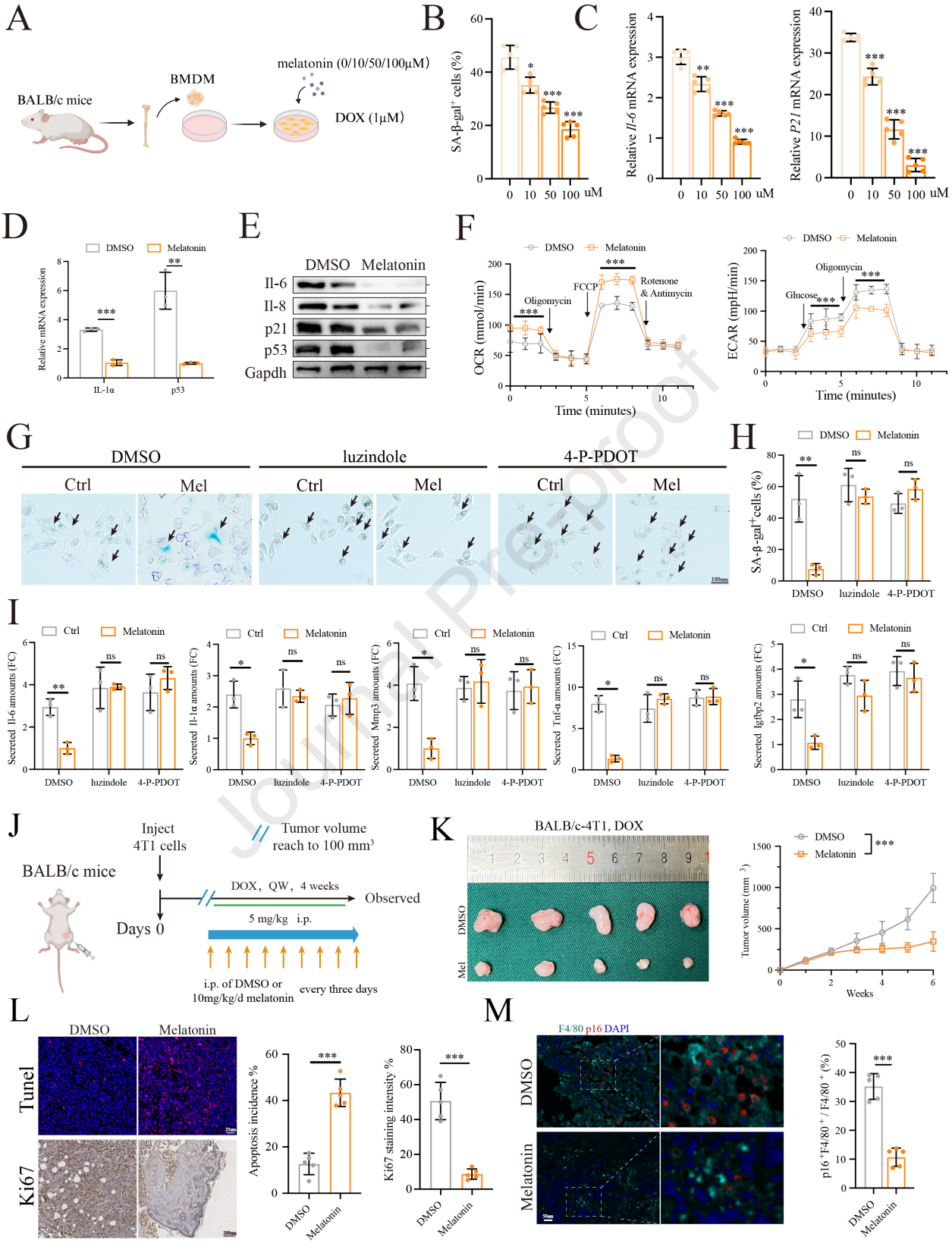

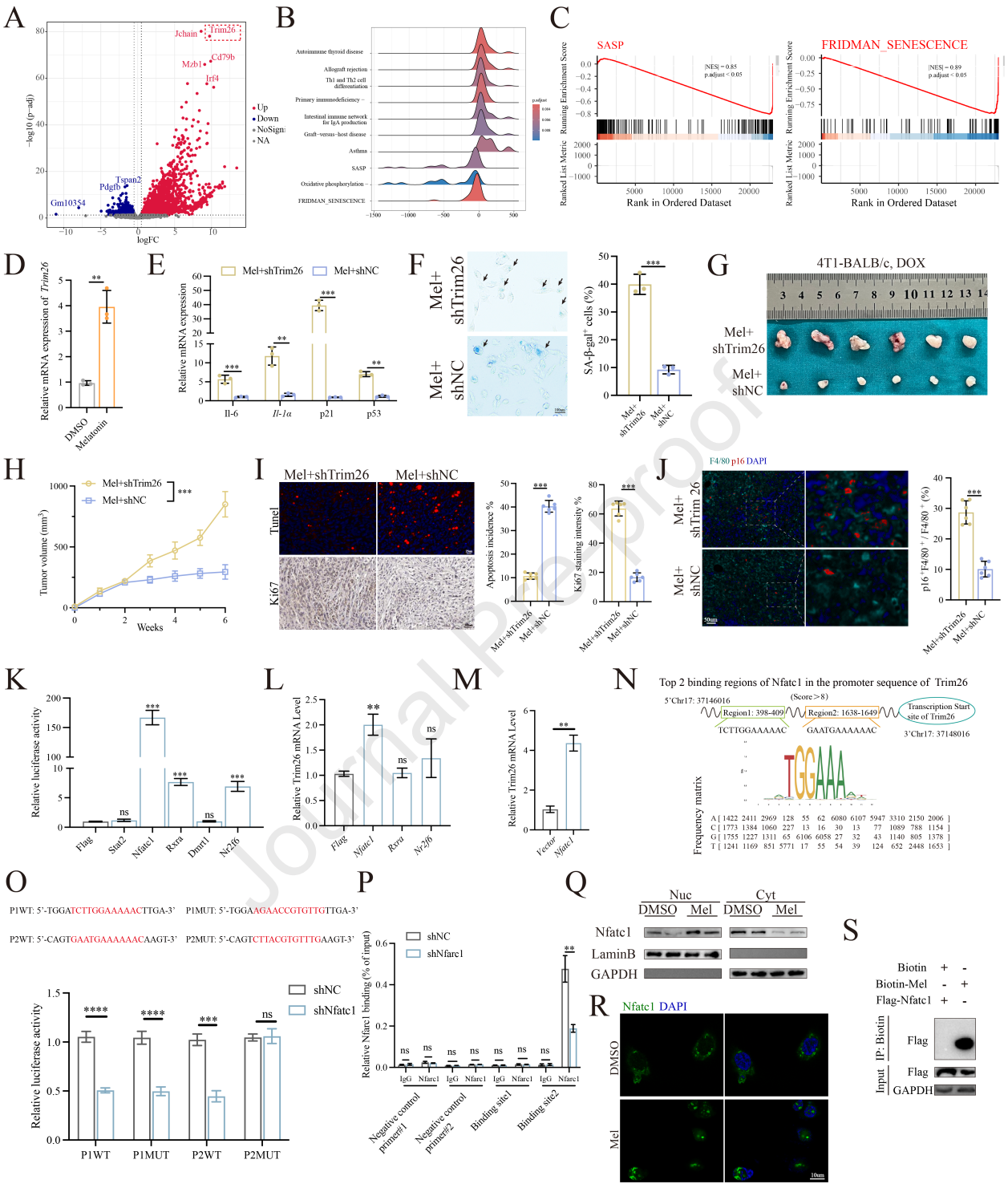

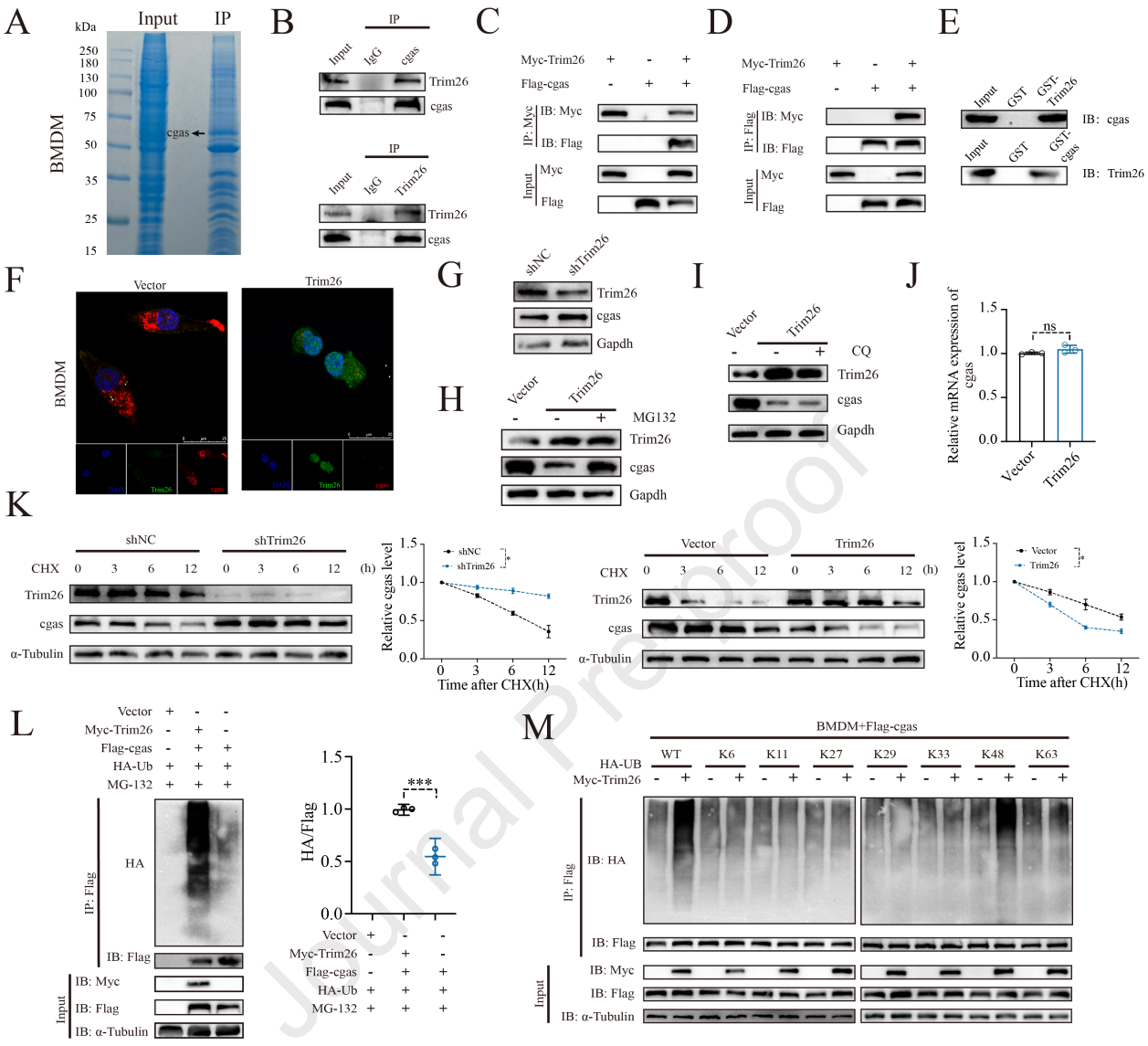

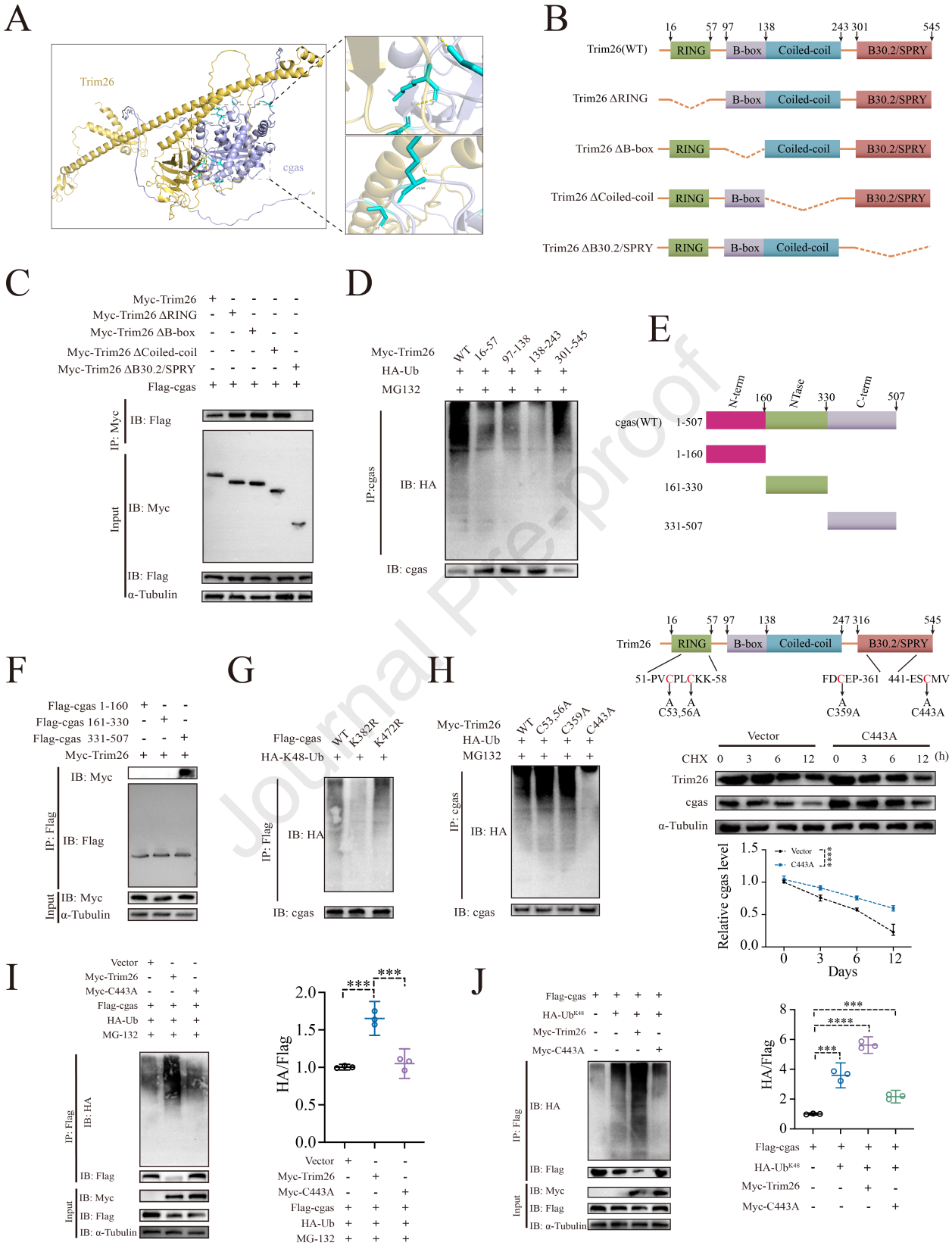
A
Trim26
cgas
B
Trim26(WT)
Trim26 ΔRING
Trim26 ΔB-box
Trim26 ΔCoiled-coil
Trim26 ΔB30.2/SPRY
RING
B-box
Coiled-coil
B30.2/SPRY
C
Myc-Trim26
Myc-Trim26 ΔRING
Myc-Trim26 ΔB-box
Myc-Trim26 ΔCoiled-coil
Myc-Trim26 ΔB30.2/SPRY
Flag-cgas
IP: Myc
IB: Flag
Input
IB: Myc
IB: Flag
α-Tubulin
D
Myc-Trim26
HA-Ub
MG132
WT
16-57
97-138
138-243
301-545
IP:cgas
IB: HA
IB: cgas
E
N-term
NTase
C-term
cgas(WT)
1-507
1-160
161-330
331-507
F
Flag-cgas 1-160
Flag-cgas 161-330
Flag-cgas 331-507
Myc-Trim26
IP: Flag
IB: Myc
IB: Flag
Input
IB: Myc
α-Tubulin
G
Flag-cgas
HA-K48-Ub
WT
K382R
K472R
IP: Flag
IB: HA
IB: cgas
H
Myc-Trim26
HA-Ub
MG132
WT
C53,56A
C359A
C443A
IP: cgas
IB: HA
IB: cgas
Trim26
51-PVCPLCKK-58
FDCEP-361
441-ESCMV
C53,56A
C359A
C443A
Vector
C443A
CHX
0 3 6 12 0 3 6 12 (h)
Trim26
cgas
α-Tubulin
Relative cgas level
Vector
C443A
Days
I
Vector
Myc-Trim26
Myc-C443A
Flag-cgas
HA-Ub
MG-132
IP: Flag
IB: HA
IB: Flag
Input
IB: Myc
IB: Flag
IB: α-Tubulin
HA/Flag
J
Flag-cgas
HA-Ub^K48
Myc-Trim26
Myc-C443A
IP: Flag
IB: HA
IB: Flag
Input
IB: Myc
IB: Flag
IB: α-Tubulin
HA/Flag

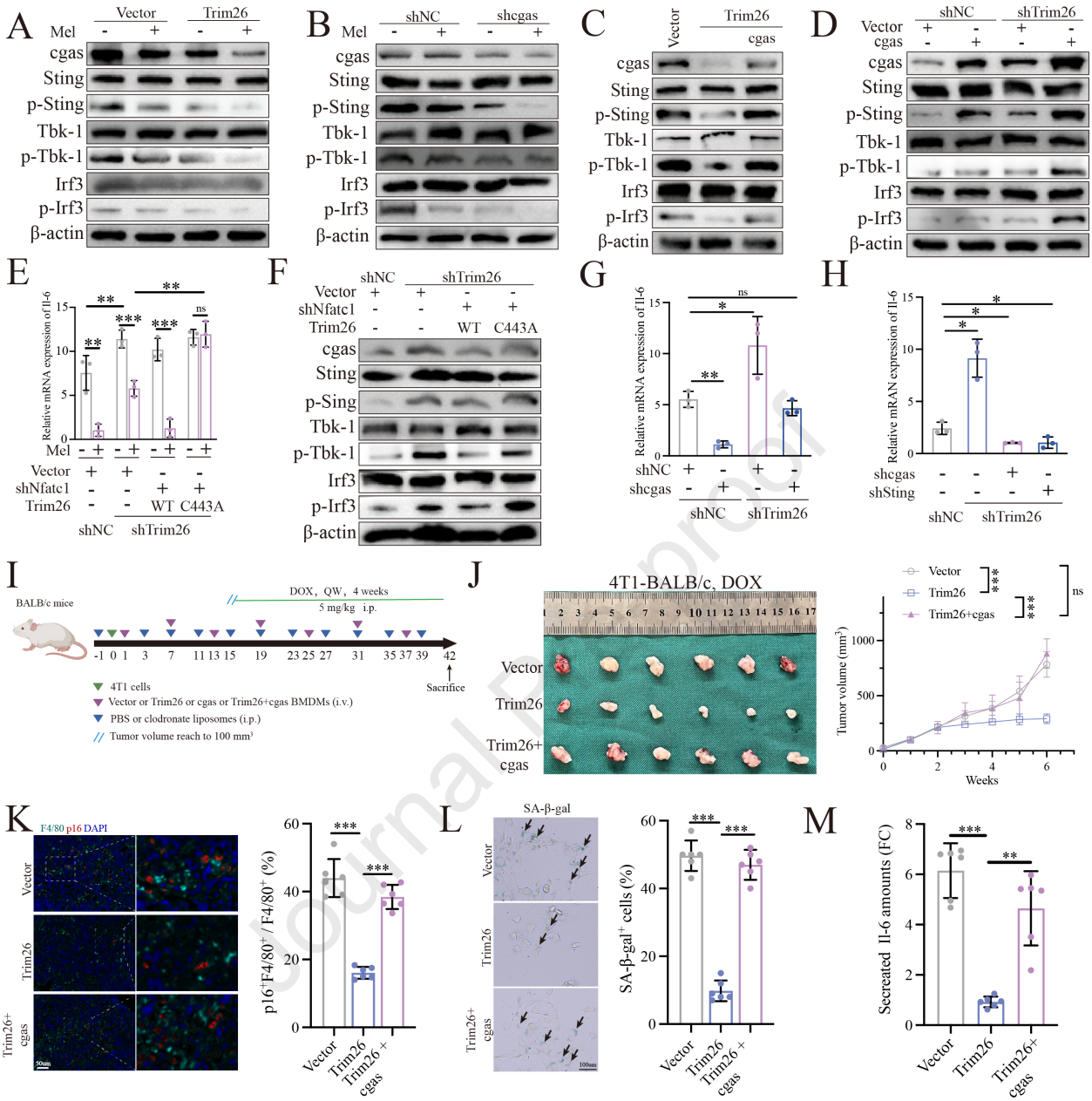
A
Mel
Vector
Trim26
cgas
Sting
p-Sting
Tbk-1
p-Tbk-1
Irf3
p-Irf3
β-actin
B
shNC
shcgas
C
D
shTrim26
E
Relative mRNA expression of Il-6
shNfatc1
WT
C443A
F
p-Sing
G
H
shcgas
shSting
I
BALB/c mice
DOX, QW, 4 weeks
5 mg/kg i.p.
Sacrifice
4T1 cells
Vector or Trim26 or cgas or Trim26+cgas BMDMs (i.v.)
PBS or clodronate liposomes (i.p.)
Tumor volume reach to 100 mm³
J
4T1-BALB/c, DOX
Trim26+ cgas
Tumor volume (mm³)
Weeks
K
F4/80 p16 DAPI
p16⁺F4/80⁺ / F4/80⁺ (%)
L
SA-β-gal
SA-β-gal⁺ cells (%)
M
Secreated Il-6 amounts (FC)

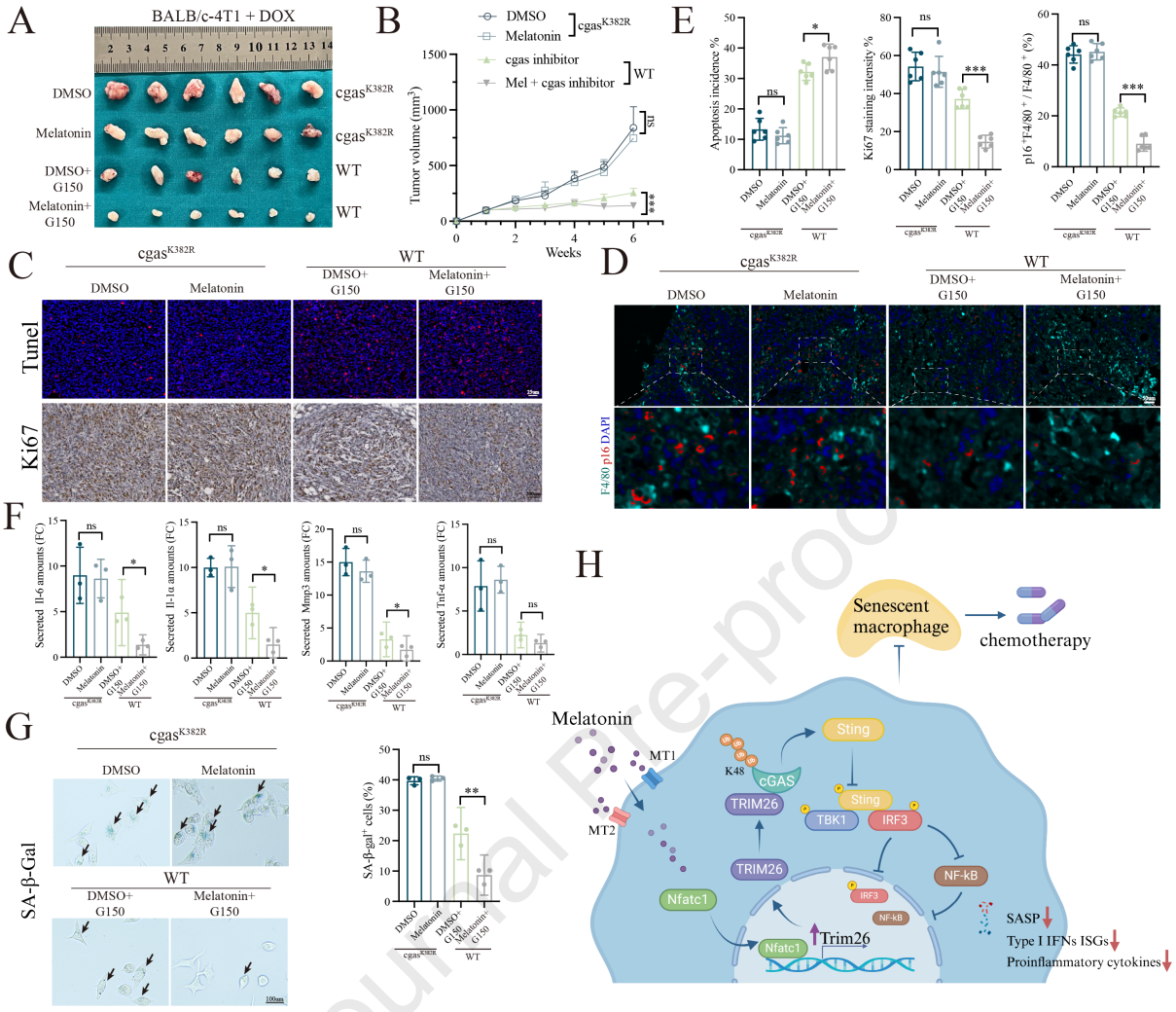
A
BALB/c-4T1 + DOX
DMSO
Melatonin
DMSO+ G150
Melatonin+ G150
cgasK382R
cgasK382R
WT
WT
B
DMSO
Melatonin
cgas inhibitor
Mel + cgas inhibitor
cgasK382R
WT
Tumor volume (mm3)
Weeks
ns
***
E
Apoptosis incidence %
Ki67 staining intensity %
p16+F4/80+ / F4/80+ (%)
ns
*
***
C
cgasK382R
WT
DMSO
Melatonin
DMSO+ G150
Melatonin+ G150
Tunel
Ki67
D
F4/80 p16 DAPI
F
Secreted Il-6 amounts (FC)
Secreted Il-1α amounts (FC)
Secreted Mmp3 amounts (FC)
Secreted Tnf-α amounts (FC)
G
SA-β-Gal
SA-β-gal+ cells (%)
**
H
Senescent macrophage
chemotherapy
Melatonin
MT1
MT2
K48
cGAS
Sting
TRIM26
TBK1
IRF3
NF-kB
Nfatc1
Trim26
SASP
Type I IFNs ISGs
Proinflammatory cytokines

The authors declare that the research was conducted in the absence of any commercial or financial relationships that could be construed as a potential conflict of interest.